Hydrogen-driven boron nitride phase differentiation during the epitaxial nucleation on the diamond (001) surface

Ting Cheng[1], Ksenia V. Bets[1], Boris I. Yakobson[1,2*]

[1] Department of Materials Science & NanoEngineering, Rice University, Houston, Texas 77005, United States

[2] Department of Chemistry, Rice University, Houston, Texas 77005, United States

*Address correspondence to: biy@rice.edu

Abstract

Cubic boron nitride (cBN) and diamond, sharing identical lattice structures, currently garner significant interest for next-generation high-power, high-frequency electronics. Despite successful heteroepitaxial synthesis of single-crystal cBN on diamond substrates via chemical vapor deposition (CVD), limited understanding of cBN growth blurs the origin of mixed BN phases under some synthesis conditions. Here, employing first-principles calculations based on a nanoreactor scheme, we study the cBN epitaxial nucleation on the diamond (001) surface under a limited-H condition. The discovered mechanism is initiated by inserting BN units into the surface dimer bond, leading to an island formation, which initially expands laterally - along the diamond surface - but rapidly switches to out-of-plane 3-dimensional growth. A high reaction barrier on the surface (~0.4-0.8 eV, 1300 K) aligns with challenging nucleation observed in experiments. Examining the environment hydrogen concentration effect revealed the origin of diverse BN phases experimentally, *i.e.*, hydrogen deficiency favors amorphous BN (aBN) growth, whereas excessive hydrogen significantly raises sp^2 bonding fraction, resulting in hexagonal BN (hBN) layers. Our results offer valuable guidance for the controllable synthesis of BN phases and advance research toward potential cBN electronics.

Introduction

Cubic boron nitride (cBN) and diamond have attracted significant interest due to their unique properties. The ultrahigh thermal conductivity - one magnitude higher than typical next-generation semiconductors like GaN and SiC - superhardness, and ultrawide bandgap make them promising candidates for next-generation high-power and high-frequency electronics.[1–5] Notably, improved *n*- and *p*-type doping in cBN compared to diamond facilitates the creation of *p*-*n* junctions.[6] However, a reliable and scalable synthesis of wafer-sized, high-quality crystals prerequisite for use in electronics is yet to be achieved for cBN. The concurrent formation of multiple phases, mostly amorphous BN (aBN), sp^2-bonded hexagonal BN (hBN) and turbostratic BN (tBN), and sp^3-bonded cBN, poses a significant obstacle,[7–10] calling for the investigation of the underlying mechanisms.

The successful synthesis of single-crystal cBN was demonstrated through several methods using diamond as a convenient heteroepitaxial substrate.[7,10–16] Molecular beam epitaxy (MBE) and physical vapor deposition (PVD) approach in the absence of hydrogen typically produce aBN followed by cBN formation. Commonly employed etching of aBN through ion bombardment leaves behind a pure cBN phase, which, unfortunately, is plagued by poor crystallinity, high defect density, and internal stress caused by high-energy ions.[8,11,13,15] The high-pressure high-temperature (HPHT) technique, typically conducted at 5-6 GPa and 1600-2000 K, offers improved quality but is limited in achievable crystal size.[12] The plasma-enhanced chemical vapor deposition (PECVD) leverages surface chemistry to improve the growth process, avoiding ion-bombardment necessity and eliminating strict high-pressure requirements. The addition of fluorine in relatively mild growth conditions (fraction of ambient pressure, 1000-1300 K) leads to the formation of pure cBN or mixed with the hBN phase by adjusting the H/F ratio.[7,10,14] Notably, PECVD also serves as a mainstream method of diamond growth for electronics applications. Significant efforts have been devoted to understanding the surface CVD diamond growth mechanism, resulting in a theoretical model of carbon addition, either by insertion into the surface dimer bond (a dimer-opening mechanism) or across the trough site between rows of dimer bonds (a trough-briding mechanism, see dimer and trough site in **Fig. 1a**).[17–20] In sharp contrast, understanding the CVD cBN epitaxy mechanism on diamonds has remained elusive for decades.

Below, we investigate the epitaxial nucleation of pure cBN on a diamond (001) surface under limited-H conditions mimicking fluorine chemistry utilized in PECVD and probe early nucleation scenarios through detailed first-principles calculations based on a nanoreactor

scheme,[21] allowing us to trace a step-by-step atomistic nucleation sequence and corresponding energy changes. Appending the nanoreactor approach with kinetic consideration, we compare reaction barriers for cBN crystal formation on various sites on the diamond surface and BN island in the early stages of growth, explaining the nucleation difficulty observed in experiments. Recognizing the importance of the environment hydrogen concentration in the cBN growth, we study its effects on the nucleation, revealing the origins of the experimentally observed mixed BN phases. This work contributes to a comprehensive atomistic understanding of cBN epitaxial nucleation on diamond, influenced by the hydrogen environment. It elucidates experimental results on diverse BN phase syntheses under specific conditions.

Results and Discussion

Methodology and diamond surface model. The well-developed nanoreactor methodology based on the step-flow crystal growth model[21] provides a comprehensive technique for investigating the nucleation sequence and energetics. On each step, a single building unit is added to the growing material, producing a range of possible structures based on various active sites. The optimal, lowest energy configuration is then identified from multiple metastable configurations and propagated as an initial configuration for the next growth or nucleation step.

To ensure the possibility of defect-free crystal formation, we assume a 1:1 ratio between supplied B and N atoms and adopt the BN dimer as the representative building unit. The direct epitaxial growth of cBN on the diamond substrate without the inclusion of hBN and tBN was successfully realized experimentally through the use of fluorine chemistry (N_2-BF_3-H_2 as the reaction gas) in PECVD synthesis[9,10,14] owing to the hydrogen-mediating ability. To mimic such an environment, we use the BNH as an immediate feeding species - the molecule undergoing direct reaction with the edge of the expanding flake or island - providing a limited amount of H (referred to as “limited-H case” in this work). It should be noted that other species should yield the same product considering the selective H atom abstraction contributed by active radicals $F^{\cdot}$, $H^{\cdot}$, $NH^{\cdot}$, $BF^{\cdot}$, *etc.*, in the plasma environment.

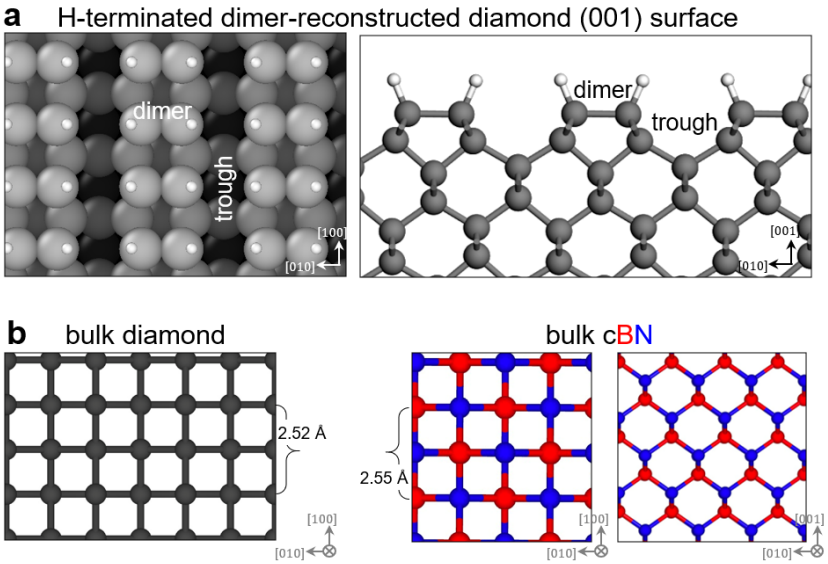

Fig. 1. a, H-terminated dimer-reconstructed diamond (001) surface. The surface dimer and trough (between dimer rows) sites are marked. The different layers of carbon surface (left) were distinguished by the gray-level in the [001] direction. **b,** Lattice comparison between diamond (left) and cBN (right). Gray, white, red, and blue balls represent C, H, B, and N atoms, respectively.

Bulk diamond and cBN share an identical lattice structure, both adopting a cubic crystal lattice arrangement, with each atom bonded to four neighboring atoms (**Fig. 1b**). A close lattice matching (~1.2% mismatch) ensures relatively low interfacial energy and good epitaxial alignment.[9] In exploring BN growth on diamond substrates, we adopt the low-index (001) diamond surface, most commonly used for heteroepitaxial cBN growth. In a typical hydrogen-rich growth environment, the surface is terminated with H atoms and exhibits its well-known stable 2 × 1 dimer-reconstruction phase characterized by forming dimer rows isolated by surface "troughs" (**Fig. 1a**).

The steps and kinks on the substrate surface are known to serve as the nucleation site, significantly lowering the nucleation barrier, as reported in experiments.[7,22] While both single- and double-layer steps are observed on this surface, we focus on the double-layer steps due to their prevalence on the vicinal substrate surface and their ability to avoid antiphase disorder in principle, which is a key concern in the epitaxial binary films. Steps on the (001) surface are separated into A and B types, corresponding to the steps running perpendicularly and parallel to the dimer row, respectively.[23] Further differentiation is made among A-steps based on the edge position compared to the nearby dimer row.[23,24] Energy comparison between three step types, *i.e.*, one B-type double-

layer steps D_B and two D_A types (**Fig. 2a-c**), on the (001) diamond surfaces indicates a preference towards D_A types (**Fig. S1**), in agreement with the observation of D_A-type steps on diamond (001) surfaces during hydrogen plasma annealing.[25] Yet high temperatures in the experiment would not allow the complete exclusion of any type, prompting us to compare the initial nucleation process on all three steps.

Employing the nanoreactor approach, we obtain the early nucleation sequence corresponding to forming the first BN row on D_A I, D_A II, and D_B steps (**Fig. 2a-c**). **Fig. 2d** depicts the corresponding energy change at $\Delta\mu_{H\_H2} = \Delta\mu_{H\_BNH} = 0$, $\Delta\mu_{BN} = 0$, along with the atomistic configuration at $N_{BNH} = 4$. In all three cases, the new BNH unit is preferentially inserted into the surface dimer bond, similar to the "dimer-opening mechanism" in the homoepitaxial diamond.[17,20] Interestingly, only the first added BNH unit forms a bond with the kink site on the diamond surface (**Fig. S2**), while the rest of the BN row follows the surface dimer row regardless of the relative step edge orientation (*i.e.*, step type), in striking contrast with the "kink-flow" mechanism for graphene or hBN nucleation on metal surfaces.[21,26,27] Despite some structural similarities, the energy trend indicates a significantly improved nucleation rate on D_A I steps (blue curve, **Fig. 2d**) compared to that of the D_B and D_A II step types (red and cyan curves, **Fig. 2d**), prompting us to focus the investigation of the following nucleation stages on D_A I only.

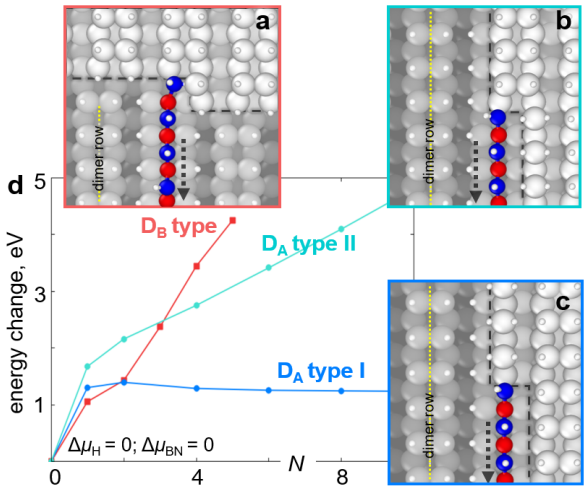

Fig. 2. **a-c,** Lowest energy configurations after adding 4 BNH species on three step types (D_B, D_A I, D_A II). Gray arrows mark the propagating direction of the new BN row. **d,** The energy change *versus* the number of added BNH species N_{BNH} on surfaces decorated with D_B(red), D_A I (blue), and D_A II (cyan) type. $\Delta\mu_{BN}$ and $\Delta\mu_H$ are set as zero.

Pure cBN phase in limited-H case. We continue the nucleation sequence for cBN on the D_A I surface in a limited-H case, extending the nanoreactor approach with more BNH units (N_{BNH} = 1-76). The schematic in **Fig. 3a** outlines the nucleation and growth progression resulting in the cBN island, indicating the formation order for BN rows (1-8) as well as the sequence of BN-layer deposition ((1)-(2)). The adsorption sites on the diamond surface are labeled according to the dimer (D) or trough (T) configuration. The corresponding energy change for the entire process at $\Delta\mu_H$ = 0 eV with various $\Delta\mu_{BN}$, *i.e.*, 0 eV (black) and 1eV/BN unit (red), is shown in **Fig. 3b**, along with several key structures in **Fig. 3c-i** (see the entire configuration sequence in **Fig. S3-S9**).

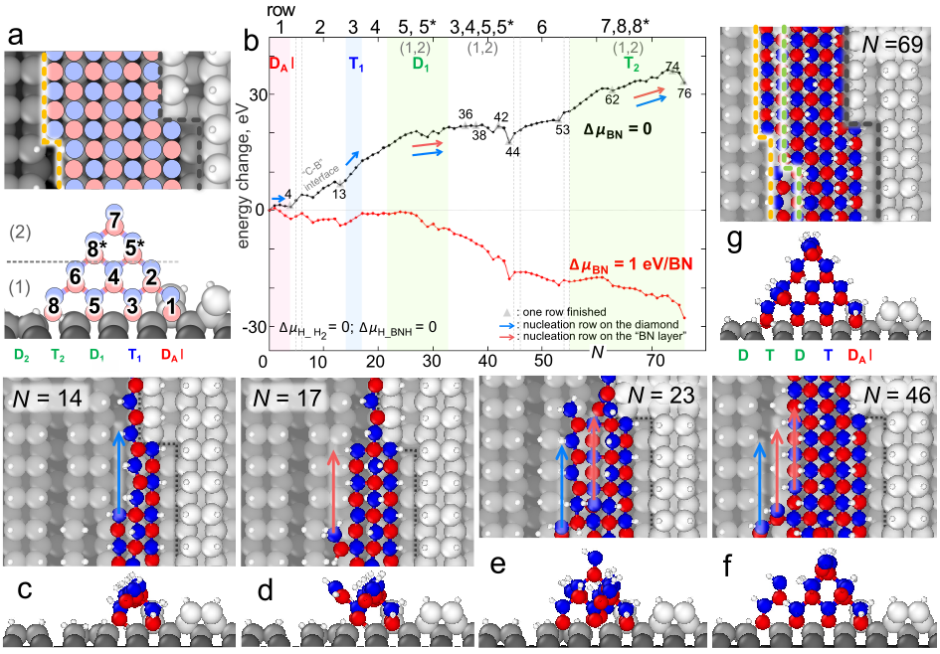

Fig. 3. **a,** Schematics of BN island formation on diamond D_A I surface. Dimer (D) and trough (T) sites of the diamond surface are marked, with nucleating BN layers ((1)-(2)) and nucleation sequences (rows 1-8) indicated. **b,** The energy change *versus* the number of added BNH species N_{BNH} at various $\Delta\mu_{BN}$, *i.e.*, 0 eV (black) and 1 eV/BN unit (red). $\Delta\mu_H$ is set as zero. The nucleation of BN layers and sequence are indicated at the top. **c-g,** Lowest energy configurations at various numbers of added BNH species. The propagation on the diamond surface and the "BN layer" are marked by blue and red arrows, respectively.

As discussed above, the BN island nucleates next to the kink on the diamond surface and immediately propagates along the dimer row of D_A I (row 1 in **Fig. 3a**). Interestingly, the next available surface sites along T_1 trough are less favorable than those directly connected to the existing row of BN atoms. Accordingly, row 2 covers completely the diamond step edge ("C-B"

interface in **Fig. 3b**, see details in **SI**), with row 3 reconnecting suspended BN atoms to the diamond T_1 surface site (**Fig. 3c**). Row 4 forms similarly to row 2 (**Fig. 3d**), eventually forming a connection to the D_1 surface site through the beginning of row 5. At this stage, as shown in **Fig. 3e**, the BN structure concurrently expands both laterally (row 5 on the D_1 surface site, layer (1)) and normally (row 5* in layer (2)) to the diamond surface, as indicated by blue and red arrows in **Fig. 3b**, respectively. Rows 6 and 7 (**Fig. 3f**) form similarly to row 4, followed by the concurrent formation of rows 8 and 8* propagating both the first and second BN layers. Each row formation, both on the diamond surface and on previously formed "BN layers", follows the kink flow mechanism – row nucleation followed by kink propagation – resulting in a repeating growth pattern (**Fig. 3g** highlights kinks on the substrate edge, first and second layers of cBN).

The observed growth sequence shows initial island expansion along the substrate surface, predominantly following the direction of the edge and dimer rows on the reconstructed diamond surface. The corrugated configuration of each cBN layer rapidly leads to the 3D growth in the direction perpendicular to the basal plane. Moreover, we found that nucleation at the D_A I site (light-red shaded area, **Fig. 3b**) is thermodynamically more favorable than the T_1 site (light-blue shaded area, **Fig. 3b**) where the energy change slope is steeper. To determine the kinetic preference of propagation along the diamond surface compared to that on top of the previously formed BN layer, we performed constrained AIMD simulations with a "slow-growth" enhanced sampling (SG-AIMD) approach at 1300 K for several key steps (**Fig. S10**). It indicates that the adsorption barrier on the surface is significantly higher (~0.8 eV for D_A I and ~0.4 eV for T_1 diamond sites, compared to 0-0.1 eV on top of "BN layer"), explaining the difficulty of the initial nucleation process on the diamond surface observed in experiments.[7,11,14]

Crystal growth is practically realized under conditions where $\Delta\mu_{BN} > 0$, ensuring sufficient speed of growth. Furthermore, the environment is often tuned to modify chemical potential, allowing preferential formation of specific target products. For example, $\Delta\mu_{BN} = 1$ eV/BN (red line, **Fig. 3b**) lowers the nucleation barrier to ~0.5 eV, favoring the overall growth process. It must be mentioned that in this example, only the chemical potential of BN units was modified while $\Delta\mu_{H\_H2}$ was kept constant. In a more realistic system, $\Delta\mu_{H\_H2}$ should also play a significant role both in energy profile and preferred products, as we will discuss below.

Other BN phases in extreme-H case. Recognizing the importance of hydrogen concentration in cBN growth, we examine the effect on the growing BN phases in two extreme conditions: no hydrogen and rich hydrogen in the growth environment.

In the absence of hydrogen in the gas phase, we expect H atoms terminating the diamond to be removed due to a high growth temperature (above 1100 K) significantly altering the BN adsorption sequence. As presented in **Fig. 4a**, the first BN unit attaches to the kink site, followed by the adsorption of new BN unit at the surface D sites without a strong preference for the site position or BN orientation (**Fig. 4b-c**). The presence of oppositely oriented BN units inhibits the ability to form a coherent crystalline phase, resulting in aBN growth. This implies that the hydrogen environment that leads to diamond surface passivation is essential for minimizing the B-B or N-N bonding during nucleation. Notably, aBN is commonly observed in the PVD[8,10] and pulsed laser deposition,[28] in which no H is included in the growth atmosphere.

In the H-rich case, the diamond surface is fully terminated by H atoms, and dangling bonds at the nucleus edge are always saturated (**Fig. 4d-f**). This leads to a reduction in sp^3-bonding between the BN nucleus and diamond surface, favoring instead adsorption of new BN units on the edge of forming BN flake, significantly increasing the sp^2 bonding fraction, which agrees well with a number of experimental findings.[7,10,14,29] In good agreement with our findings, small tilted pure hBN domains directly on diamond (001) surface have been realized by rich hydrogen gas in a recent experiment.[29]

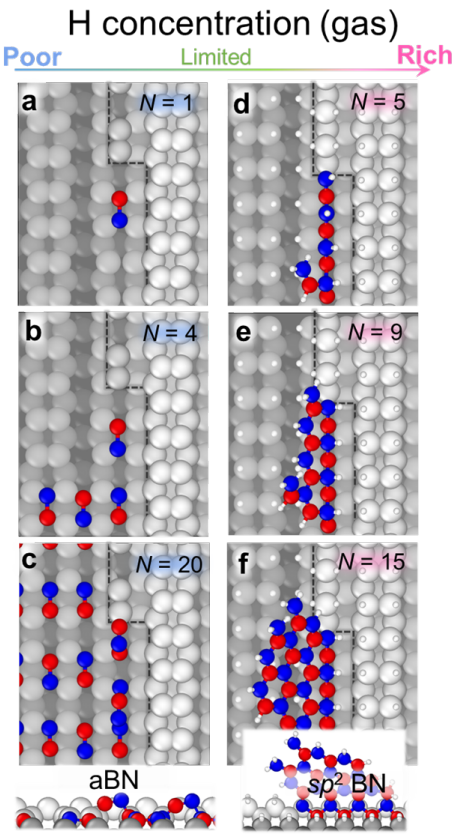

Fig. 4. Optimal sample configurations with labeled number of added BNH species N_{BNH} during the nucleation on diamond D_A I surface when included **a-c,** no hydrogen or **d-f,** excessive hydrogen in the growth environment. No hydrogen (blue, poor-H case) present in the gas phase tends to form aBN (inset of (c)), while the excess of hydrogen concentration (pink, rich-H case) significantly increases the sp^2 bonding fraction of BN (inset of (f)).

To quantify the effect of the environment H concentration on the BN product (hBN and cBN), we vary the $\Delta\mu_{H\_H2}$ term (keep $\Delta\mu_{BN}$= 0 and $\Delta\mu_{H\_BNH}$= -0.2 eV constant) and plot the critical nucleation barrier for limited-H (green line) and rich-H (pink line) case in **Fig. 5a**. The inset of **Fig. 5a** provides an example of the energy change during the nucleation for both cases, clearly showing their respective critical barrier at $\Delta\mu_{H\_H2}$ = -1.6 eV/atom. We find that the change in $\Delta\mu_{H\_H2}$ value alters the preferred BN phase. The sp^2-bonded hBN is more favorable (let barrier difference between two phases is above 1 eV) at $\Delta\mu_{H\_H2} > -1.45$ eV (light-pink shaded area, **Fig. 5a**), while the cBN phase dominates at $\Delta\mu_{H\_H2} < -1.55$ eV (*i.e.*, a limited hydrogen flow), marked by light-green shaded area in **Fig. 5a**. Note that the upper-boundary ($\Delta\mu_{H\_H2}$ = -0.8 eV) for sp^2 BN phase in **Fig. 5a** is determined by the typical experimental conditions ($T > 1000$ K, $P_{H2} < 10^2$ Torr). Interestingly, the critical nucleation barrier for the limited-H case producing cBN phase gradually

reduces as $\Delta\mu_{H\_H2}$ decreases. This suggests a limited hydrogen reaction (that is, mixed H_2 with a H_2-consuming gas, *e.g.*, BF_3) minimizes the sp^2 bonding of the BN nanomaterials during the nucleation, explaining the importance of H/F ratio in the "fluorine chemistry" experiments to obtain pure cBN.[7,10,14] According to the H chemical potential, we produce an approximate phase diagram of experimental conditions and the corresponding dominant BN phase (**Fig. 5b**). Typical experimental data (red dot, **Fig. 5b**) are consistent with our calculated phase. It shows the cBN phase favors a lower H_2 pressure at a given temperature, while hBN dominates when H_2 pressure is higher.

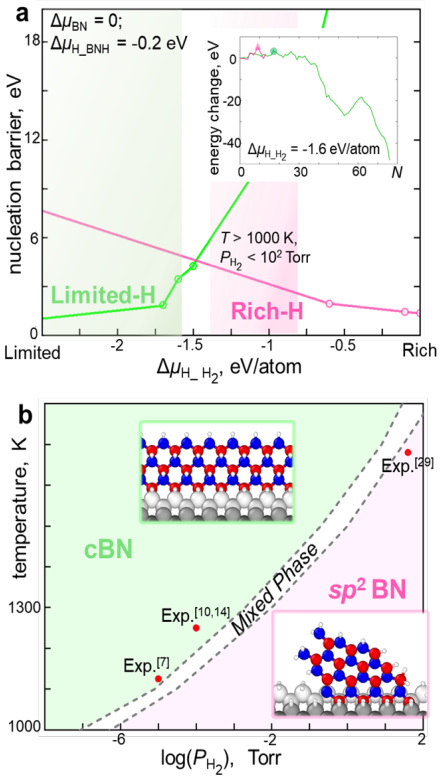

Fig. 5. a, Nucleation barrier *versus* H chemical potential $\Delta\mu_{H\_H2}$ during the nucleation for limited-H (green) and rich-H (pink) case. $\Delta\mu_{BN} = 0$, and $\Delta\mu_{H\_BNH}$ = -0.2 eV. The light-shaded area marks the experimental conditions ($T > 1000$ K, $P_{H2} < 10^2$ Torr) in which phase dominates, colored by their phase type. Inset: an example of energy change curves for two cases at $\Delta\mu_{H\_H2} = -1.6$ eV/atom. The critical nuclei for limited-H (green circle) and rich-H (pink triangle) cases are $N = 17$ and $N = 9$, respectively. **b**, Calculated phase diagram between cBN and sp^2 BN phase, related to H_2 pressure and temperature. Left and right inset: front side view of the representative product in these two cases. Red points denote the experimental results from references[7,10,14,29].

One can leverage the above result to theoretically guide the controllable synthesis of pure BN phases. Generally, in ambient pressure, sp^2-bonded hBN or tBN is more commonly observed than sp^3-bonded cBN phase, which is preferred in HPHT conditions.[30] Yet diamond substrate provides an identical cubic crystal lattice with close lattice-matching for cBN, promoting the formation of sp^3-bonded BN over other BN phases on this surface without a strict high-pressure requirement. However, a fully passivated diamond dimer-reconstructed surface gives a challenging initial nucleation of BN. Therefore, first, a clean diamond surface with steps/kinks is a crucial prerequisite to provide active nucleation sites for the cBN phase. Importantly, double-layer steps, which occur predominantly on vicinal diamond surfaces with high step density, are a good choice to induce single-domain growth,[23] while single-layer steps cause antiphase boundary formation typically observed in synthesizing III-IV semiconductors on the silicon substrate.[31] Second, because of the non-catalytic properties of the diamond surface, the growth should provide enough BN species in the gas phase, usually utilizing plasma or microwave technology to avoid high decomposition barriers[32], ensuring a building unit addition-limited, not surface-diffusion-limited process. Last, the hydrogen environment is crucial to controlling the BN phase on the diamond. In the initial growth stage, H atoms act as terminating species to help uphold the heteroepitaxial cubic BN-layer formation and minimize the B-B or N-N bonding, avoiding aBN formation. Yet, excessive H atoms saturating the BN edge yield the sp^2-bonded BN production. Thus, using H_2-consuming gas (*e.g.*, BF_3) mixed with H_2 is vital to adjust the H concentration in the atmosphere to selectively produce the cBN phase on diamonds.

Conclusions

In summary, inspired by the successful experimental epitaxial growth of pure cBN film on a diamond substrate using the CVD technique, we have probed its feasibility and early nucleation scenarios through detailed first-principles calculations based on a nanoreactor scheme, which follows step-flow crystal growth theory. The atomic row assembly and energy levels are tractable in a step-by-step diagram. It shows that the local kink/step of diamond surface facilitates the nucleation of initial "BN" feeding species along the surface dimer row orientation independent of the step edge direction.

Under a limited H condition, we determine that the barrier for cBN phase nucleation on the diamond surface with kink is ~0.5 eV at moderate nonequilibrium dynamics (*e.g.*, $\Delta\mu_{BN}$ = 1eV/BN).

The overall nucleation sequence initiates on a diamond surface (T and D sites), expanding in-plane but rapidly switching to out-of-plane 3D growth. Our results highlight that nucleation at the surface D site is thermodynamically more favorable than the T site. Still, both necessitate overcoming a higher kinetic barrier than on the "BN layer" (0.4-0.8 eV *vs* 0-0.1 eV at 1300 K via SG-AIMD), yielding challenging nucleation in the early stage, as evidenced in experiments.

Two extreme cases (*i.e.*, poor-H and rich-H) are also studied. Hydrogen is essential for minimizing the B-B or N-N bonding during nucleation, leading to aBN formation in the poor-H case. On the other hand, an abundance of hydrogen in the atmosphere significantly increases the sp^2 bonding fraction of BN nanomaterials, with the cBN phase emerging prominently only under limited hydrogen flow ($\Delta\mu_{H\_H2} < -1.55$ eV). These insights contribute to a comprehensive atomistic understanding of cBN epitaxy nucleation on the diamond, elucidating experimental results on diverse BN phase syntheses on diamond surfaces, further serving as a guide for experiments, and advancing research toward potential device applications.

References

(1) Tian, Y.; Xu, B.; Yu, D.; Ma, Y.; Wang, Y.; Jiang, Y.; Hu, W.; Tang, C.; Gao, Y.; Luo, K.; Zhao, Z.; Wang, L.-M.; Wen, B.; He, J.; Liu, Z. Ultrahard Nanotwinned Cubic Boron Nitride. *Nature* **2013**, *493* (7432), 385–388. https://doi.org/10.1038/nature11728.

(2) Chen, K.; Song, B.; Ravichandran, N. K.; Zheng, Q.; Chen, X.; Lee, H.; Sun, H.; Li, S.; Udalamatta Gamage, G. A. G.; Tian, F.; Ding, Z.; Song, Q.; Rai, A.; Wu, H.; Koirala, P.; Schmidt, A. J.; Watanabe, K.; Lv, B.; Ren, Z.; Shi, L.; Cahill, D. G.; Taniguchi, T.; Broido, D.; Chen, G. Ultrahigh Thermal Conductivity in Isotope-Enriched Cubic Boron Nitride. *Science* **2020**, *367* (6477), 555–559. https://doi.org/10.1126/science.aaz6149.

(3) Gong, Y.; Luo, D.; Choe, M.; Kim, Y.; Ram, B.; Zafari, M.; Seong, W. K.; Bakharev, P.; Wang, M.; Park, I. K.; Lee, S.; Shin, T. J.; Lee, Z.; Lee, G.; Ruoff, R. S. Growth of Diamond in Liquid Metal at 1 Atm Pressure. *Nature* **2024**, 1–7. https://doi.org/10.1038/s41586-024-07339-7.

(4) Tsao, J. Y.; Chowdhury, S.; Hollis, M. A.; Jena, D.; Johnson, N. M.; Jones, K. A.; Kaplar, R. J.; Rajan, S.; Van de Walle, C. G.; Bellotti, E.; Chua, C. L.; Collazo, R.; Coltrin, M. E.; Cooper, J. A.; Evans, K. R.; Graham, S.; Grotjohn, T. A.; Heller, E. R.; Higashiwaki, M.;

Islam, M. S.; Juodawlkis, P. W.; Khan, M. A.; Koehler, A. D.; Leach, J. H.; Mishra, U. K.; Nemanich, R. J.; Pilawa-Podgurski, R. C. N.; Shealy, J. B.; Sitar, Z.; Tadjer, M. J.; Witulski, A. F.; Wraback, M.; Simmons, J. A. Ultrawide-Bandgap Semiconductors: Research Opportunities and Challenges. *Adv. Electron. Mater.* **2018**, *4* (1), 1600501. https://doi.org/10.1002/aelm.201600501.

(5) Chilleri, J.; Siddiqua, P.; Shur, M. S.; O'Leary, S. K. Cubic Boron Nitride as a Material for Future Electron Device Applications: A Comparative Analysis. *Appl. Phys. Lett.* **2022**, *120* (12), 122105. https://doi.org/10.1063/5.0084360.

(6) Mishima, O.; Tanaka, J.; Yamaoka, S.; Fukunaga, O. High-Temperature Cubic Boron Nitride P-N Junction Diode Made at High Pressure. *Science* **1987**, *238* (4824), 181–183. https://doi.org/10.1126/science.238.4824.181.

(7) Brown, J. M.; Vishwakarma, S.; Smith, D. J.; Nemanich, R. J. Nucleation of Cubic Boron Nitride on Boron-Doped Diamond via Plasma Enhanced Chemical Vapor Deposition. *J. Appl. Phys.* **2023**, *133* (21), 215303. https://doi.org/10.1063/5.0145771.

(8) Li, Q.; Wong, S. F.; Lau, W. M.; Ong, C. W. Study of the Surface Layer in cBN Growth by PVD Techniques. *Diam. Relat. Mater.* **2007**, *16* (3), 421–424. https://doi.org/10.1016/j.diamond.2006.08.020.

(9) Zhang, W. J.; Meng, X. M.; Chan, C. Y.; Chan, K. M.; Wu, Y.; Bello, I.; Lee, S. T. Interfacial Study of Cubic Boron Nitride Films Deposited on Diamond. *J. Phys. Chem. B* **2005**, *109* (33), 16005–16010. https://doi.org/10.1021/jp0517908.

(10) Zhang, W. J.; Chan, C. Y.; Meng, X. M.; Fung, M. K.; Bello, I.; Lifshitz, Y.; Lee, S. T.; Jiang, X. The Mechanism of Chemical Vapor Deposition of Cubic Boron Nitride Films from Fluorine-Containing Species. *Angew. Chem. Int. Ed.* **2005**, *44* (30), 4749–4753. https://doi.org/10.1002/anie.200500320.

(11) Zhang, X. W.; Boyen, H.-G.; Deyneka, N.; Ziemann, P.; Banhart, F.; Schreck, M. Epitaxy of Cubic Boron Nitride on (001)-Oriented Diamond. *Nat. Mater.* **2003**, *2* (5), 312–315. https://doi.org/10.1038/nmat870.

(12) Chen, C.; Wang, Z.; Kato, T.; Shibata, N.; Taniguchi, T.; Ikuhara, Y. Misfit Accommodation Mechanism at the Heterointerface between Diamond and Cubic Boron Nitride. *Nat. Commun.* **2015**, *6* (1), 6327. https://doi.org/10.1038/ncomms7327.

(13) Hirama, K.; Taniyasu, Y.; Karimoto, S.; Krockenberger, Y.; Yamamoto, H. Single-Crystal

Cubic Boron Nitride Thin Films Grown by Ion-Beam-Assisted Molecular Beam Epitaxy. *Appl. Phys. Lett.* **2014**, *104* (9), 092113. https://doi.org/10.1063/1.4867353.

(14) Zhang, W.; Bello, I.; Lifshitz, Y.; Chan, K. M.; Meng, X.; Wu, Y.; Chan, C. Y.; Lee, S.-T. Epitaxy on Diamond by Chemical Vapor Deposition: A Route to High-Quality Cubic Boron Nitride for Electronic Applications. *Adv. Mater.* **2004**, *16* (16), 1405–1408. https://doi.org/10.1002/adma.200306658.

(15) Hirama, K.; Taniyasu, Y.; Karimoto, S.; Yamamoto, H.; Kumakura, K. Heteroepitaxial Growth of Single-Domain Cubic Boron Nitride Films by Ion-Beam-Assisted MBE. *Appl. Phys. Express* **2017**, *10* (3), 035501. https://doi.org/10.7567/APEX.10.035501.

(16) Storm, D. F.; Maximenko, S. I.; Lang, A. C.; Nepal, N.; Feygelson, T. I.; Pate, B. B.; Affouda, C. A.; Meyer, D. J. Mg-Facilitated Growth of Cubic Boron Nitride by Ion Beam-Assisted Molecular Beam Epitaxy. *Phys. Status Solidi RRL – Rapid Res. Lett.* **2022**, *16* (7), 2200036. https://doi.org/10.1002/pssr.202200036.

(17) Garrison, B. J.; Dawnkaski, E. J.; Srivastava, D.; Brenner, D. W. Molecular Dynamics Simulations of Dimer Opening on a Diamond {001}(2x1) Surface. *Science* **1992**, *255* (5046), 835–838. https://doi.org/10.1126/science.255.5046.835.

(18) Harris, S. J. Mechanism for Diamond Growth from Methyl Radicals. *Appl. Phys. Lett.* **1990**, *56* (23), 2298–2300. https://doi.org/10.1063/1.102946.

(19) Skokov, S.; Weiner, B.; Frenklach, M. Elementary Reaction Mechanism for Growth of Diamond (100) Surfaces from Methyl Radicals. *J. Phys. Chem.* **1994**, *98* (28), 7073–7082. https://doi.org/10.1021/j100079a030.

(20) Cheesman, A.; Harvey, J. N.; Ashfold, M. N. R. Studies of Carbon Incorporation on the Diamond {100} Surface during Chemical Vapor Deposition Using Density Functional Theory. *J. Phys. Chem. A* **2008**, *112* (45), 11436–11448. https://doi.org/10.1021/jp8034538.

(21) Artyukhov, V. I.; Liu, Y.; Yakobson, B. I. Equilibrium at the Edge and Atomistic Mechanisms of Graphene Growth. *Proc. Natl. Acad. Sci.* **2012**, *109* (38), 15136–15140. https://doi.org/10.1073/pnas.1207519109.

(22) Lee, S. T.; Peng, H. Y.; Zhou, X. T.; Wang, N.; Lee, C. S.; Bello, I.; Lifshitz, Y. A Nucleation Site and Mechanism Leading to Epitaxial Growth of Diamond Films. *Science* **2000**, *287* (5450), 104–106. https://doi.org/10.1126/science.287.5450.104.

(23) Chadi, D. J. Stabilities of Single-Layer and Bilayer Steps on Si(001) Surfaces. *Phys. Rev.*

Lett. **1987**, *59* (15), 1691–1694. https://doi.org/10.1103/PhysRevLett.59.1691.

(24) Tsai, M.-H.; Yeh, Y.-Y. Molecular-Dynamics Calculations of Energetics and Geometries of Steps on Diamond C(001). *Phys. Rev. B* **1998**, *58* (4), 2157–2160. https://doi.org/10.1103/PhysRevB.58.2157.

(25) Kuang, Y.; Wang, Y.; Lee, N.; Badzian, A.; Badzian, T.; Tsong, T. T. Surface Structure of Homoepitaxial Diamond (001) Films, a Scanning Tunneling Microscopy Study. *Appl. Phys. Lett.* **1995**, *67* (25), 3721–3723. https://doi.org/10.1063/1.115361.

(26) Zhang, Z.; Liu, Y.; Yang, Y.; Yakobson, B. I. Growth Mechanism and Morphology of Hexagonal Boron Nitride. *Nano Lett.* **2016**, *16* (2), 1398–1403. https://doi.org/10.1021/acs.nanolett.5b04874.

(27) Bets, K. V.; Gupta, N.; Yakobson, B. I. How the Complementarity at Vicinal Steps Enables Growth of 2D Monocrystals. *Nano Lett.* **2019**, *19* (3), 2027–2031. https://doi.org/10.1021/acs.nanolett.9b00136.

(28) Biswas, A.; Alvarez, G. A.; Li, T.; Christiansen-Salameh, J.; Jeong, E.; Puthirath, A. B.; Iyengar, S. A.; Li, C.; Gray, T.; Zhang, X.; Pieshkov, T. S.; Kannan, H.; Elkins, J.; Vajtai, R.; Birdwell, A. G.; Neupane, M. R.; Garratt, E. J.; Pate, B. B.; Ivanov, T. G.; Zhao, Y.; Tian, Z.; Ajayan, P. M. Structural, Optical, and Thermal Properties of BN Thin Films Grown on Diamond via Pulsed Laser Deposition. *Phys. Rev. Mater.* **2023**, *7* (9), 094602. https://doi.org/10.1103/PhysRevMaterials.7.094602.

(29) Yang, X.; Pristovsek, M.; Nitta, S.; Liu, Y.; Honda, Y.; Koide, Y.; Kawarada, H.; Amano, H. Epitaxial Combination of Two-Dimensional Hexagonal Boron Nitride with Single-Crystalline Diamond Substrate. *ACS Appl. Mater. Interfaces* **2020**, *12* (41), 46466–46475. https://doi.org/10.1021/acsami.0c11883.

(30) Bundy, F. P.; Wentorf, R. H., Jr. Direct Transformation of Hexagonal Boron Nitride to Denser Forms. *J. Chem. Phys.* **1963**, *38* (5), 1144–1149. https://doi.org/10.1063/1.1733815.

(31) Kroemer, H. Polar-on-Nonpolar Epitaxy. *J. Cryst. Growth* **1987**, *81* (1), 193–204. https://doi.org/10.1016/0022-0248(87)90391-5.

(32) Cheng, T.; Bets, K. V.; Yakobson, B. I. Synthesis Landscapes for Ammonia Borane Chemical Vapor Deposition of H-BN and BNNT: Unraveling Reactions and Intermediates from First-Principles. *J. Am. Chem. Soc.* **2024**, *146* (13), 9318–9325. https://doi.org/10.1021/jacs.4c01354.